Simulating Vapor−Liquid Nucleation of Water: A Combined Histogram-Reweighting and Aggregation-Volume-Bias Monte Carlo Investigation for Fixed-Charge and Polarizable Models

Bin Chen,*,† J. Ilja Siepmann,‡ and Michael L. Klein§

Department of Chemistry, Louisiana State University, Baton Rouge, Louisiana 70803-1804, Departments of Chemistry and of Chemical Engineering and Materials Science, University of Minnesota, 207 Pleasant Street S.E., Minneapolis, Minnesota 55455-0431, and Center for Molecular Modeling and Department of Chemistry, University of Pennsylvania, 231 S. 34th Street, Philadelphia, Pennsylvania 19104-6323

Received: August 11, 2004; In Final Form: October 14, 2004

The method of histogram-reweighting was integrated with a recently developed approach using aggregation-volume-bias Monte Carlo and self-adaptive umbrella sampling to develop the AVUS-HR algorithm that allows for exceedingly efficient calculations of nucleation properties over a wide range of thermodynamic conditions. Simulations were carried out for water using both fixed-charge and polarizable force fields belonging to the TIP4P family (namely, TIP4P, TIP4P−FQ, TIP4P-pol2, and TIP4P-pol3) to investigate the nucleation of water over a temperature range from 200 to 300 K and the concentration of water clusters in the atmosphere at elevations up to 15 km. It was found that the nucleation free energy barriers and atmospheric concentrations are extremely sensitive to the force field, albeit all of the models investigated in this study support the following general conclusions: (i) ice nucleation is not present under the thermodynamic conditions and cluster-size range investigated here, i.e., the critical nuclei possess liquidlike structures, and (ii) the atmospheric concentrations of water clusters under homogeneous conditions are very low with the mole fraction of hexamers being about 10^{-10}, a number probably too low to influence the solar radiation balance. Compared to the experimental data, the TIP4P-pol3 model yields the most accurate nucleation results, consistent with its excellent performance for the second virial coefficient and the minimum cluster energies.

1. Introduction

Nucleation, a fundamental first step in phase transitions, plays a critical role in many processes of environmental and technological importance. In particular, due to its relevance for environmental and atmospheric processes (e.g., its direct involvement in processes from generation of clathrate hydrates to cloud formation), nucleation/condensation of water is a topic of considerable interest that has been the central focus for a great deal of experimental investigations.[1−17] The quantitative study of this phenomenon began more than 100 years ago with the expansion chamber experiment by Wilson,[1] whereas the more recent development of nucleation pulse techniques has enabled more accurate measurements of water nucleation rates. Together these studies have shown that the nucleation rates predicted by simple macroscopic theories (such as the classical nucleation theory) cannot adequately describe the experimental results. However, nucleation experiments are very challenging and noticeable discrepancies were also found between different sets of experiments. Most importantly for water nucleation under atmospheric conditions, the latest two experimental measurements[16,17] done by two separate groups show an appreciable disagreement for the temperature-dependence of the onset water-nucleation supersaturation over the low-temperature range from 200 to 260 K. In fact, the sharp turning-point at 207 K observed by Peeters et al.[17] (but not so obvious in Wölk and Strey's data[17]) led the former group to infer a transition from vapor/liquid to vapor/solid nucleation. On the other hand, a recent simulation investigation points to quite different performances for various water force fields.[18] More interestingly, it was shown that a polarizable force field (which is supposed to achieve better transferability) does not necessarily yield better predictions for water nucleation than the nonpolarizable force fields.

In this paper, we report on a simulation study of water nucleation over a broad temperature range from 200 to 300 K. In addition to assessing more extensively the transferability of water force fields on nucleation properties and the possibility of ice nucleation at low temperatures, the homogeneous aggregation of water molecules in the atmosphere was also investigated. Interest on this subject was brought up by the recently emphasized discrepancy between the observed and calculated atmospheric absorption of solar radiation.[19] Absorption of solar radiation is believed to be an important factor in determining the Earth's temperature, weather, and climate. Water complexes could serve as a potential absorber since their spectra are significantly broadened and red-shifted compared to that of a water monomer.[20,21] Evans and Vaida[19] carried out a statistical mechanical analysis of water cluster concentrations (up to hexamers) in the atmosphere. A simple two body potential was used in their work so that an analytical expression could be obtained to allow a fast evaluation of these cluster concentrations over a wide range of altitudes (from sea-level to 15 km above). Here we show that particle-based simulations offer a better alternative for this problem since the solution is exact for a given model and more complex force fields (e.g.,

* Corresponding author. E-mail: binchen@lsu.edu.
† Louisiana State University.
‡ University of Minnesota.
§ University of Pennsylvania.

10.1021/jp0463722 CCC: $30.25 © 2005 American Chemical Society
Published on Web 01/25/2005

articulated multisite models with separate terms representing first-order electrostatic and dispersive interactions as well as second-order polarization effects) can be employed. Furthermore, by bringing the method of histogram-reweighting[22,23] into our recently developed nucleation simulation approach,[24−26] very few simulations (in fact, only two for this case) are required in order to compute the concentration of water clusters over a wide range of sizes, temperatures, and partial pressures including the set of thermodynamic conditions relevant for absorption of solar radiation.

In the next section, the technical details of the newly developed nucleation simulation approach, called AVUS-HR (combining histogram reweighting with aggregation-volume-bias Monte Carlo simulations using self-adaptive umbrella sampling) are presented. In section 3, the molecular models (force fields) and simulation conditions of this study are briefly described. The simulation results are presented and discussed in section 4, and section 5 provides concluding remarks.

2. Integration of the Histogram-Reweighting Technique

Before presenting the details of this technical integration, we briefly describe the original nucleation simulation method that led to our recent success in simulating various rare nucleation events.[24−26] This method consists of a combination of the aggregation-volume-bias Monte Carlo (AVBMC) algorithm,[27,28] the configurational-bias Monte Carlo (CBMC) scheme,[29−31] and the umbrella sampling technique.[32] Key to this method is that AVBMC swaps are introduced, which enable efficient particle transfer between the cluster and the mother phase. Unlike the random displacements used in the conventional Metropolis Monte Carlo scheme[33] and the solely force-driven diffusion employed in molecular dynamics simulations, the space surrounding a molecule is explicitly divided into associating and nonassociating regions for the AVBMC swap moves. This allows other molecules to directly hop between these two regions and thereby bypass the time and spatial constraints limiting the sampling in molecular dynamics (where the cluster growth relies on the slow diffusion process) and Metropolis Monte Carlo simulations (where cluster growth depends on fortuitous but random collisions of gas-phase molecules with the cluster). Furthermore, through its construction (i.e., the use of an asymmetric underlying transition matrix for the Markov chain), the AVBMC algorithm is able to balance the different energetic and entropic factors characteristic for transitions between the microphase regions (cluster and monomer phases) by (i) attempting, more frequently, moves that lead to lower entropy and energy (cluster formation/growth) and by (ii) enhancing the acceptance rates for moves that lead to higher entropy and energy (cluster destruction/shrinkage). Correspondingly, more efficient sampling of all the relevant microphase regions (monomers and clusters) can be achieved. The incorporation of the CBMC scheme[29−31] further improves the acceptance rates for the AVBMC swaps and most importantly allows the extension of this method to molecules with articulated structures. In addition, the probability of observing rare critical nuclei is enhanced via the umbrella sampling technique.[32] To let clusters of all sizes of interest be sampled evenly in the simulation, the umbrella potential is chosen to approach the negative of the nucleation free energy, which is solved iteratively using a self-adapting procedure.[24−26]

The integration of histogram-reweighting[22,23] into this technique further enhances its power/capability. In particular, by sorting the simulation data in the forms of histograms of fluctuating observables, the method of histogram reweighting

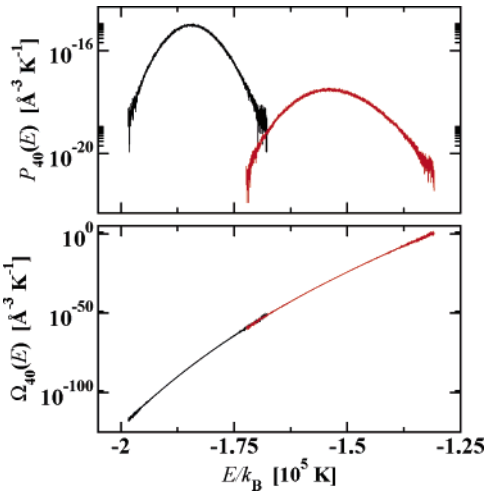

Figure 1. (Top) Energy distributions (expressed as an absolute density) for a tetracontamer (40-mer) calculated from two simulations at $T = 200$ K and $n_v = 4.93 \times 10^{-9}$ Å^{-3} (black) and $T = 300$ K and $n_v = 5.4 \times 10^{-6}$ Å^{-3} (red) using the TIP4P model. (Bottom) The corresponding density of microcanonical states as function of energy obtained at these two thermodynamic conditions.

can extract information not only for the thermodynamic state under investigation but also for other neighboring thermodynamic states *without additional simulations*. The underlying idea is that the microcanonical partition function of a given system is independent of the simulation conditions, such as temperature and chemical potential (or in other words, the system can access the same set of microcanonical states under different simulation conditions, but with different probabilities). The use of such method in our nucleation simulation approach is even more robust. First, the microcanonical partition function of a cluster with a given size n (n-mer) is a function of the energy only. Correspondingly, a simple one-dimensional histogram $\Omega_n(E)$, varied only over the energy axis, is needed to express this property, which can be conveniently constructed from the simulations as follows

$$\Omega_n(E) = P_n(E)\, e^{(-n\mu_1+E)/k_B T} \tag{1}$$

where $P_n(E)$ is the probability to observe this n-mer with energy E, μ_1 is the gas-phase (monomer) chemical potential, k_B is Boltzmann's constant, and T is the absolute temperature. Furthermore, due to the small sizes of these clusters, the energy fluctuations are typically large. Therefore, good overlaps of these histograms are expected even for a relatively wide temperature window. For example, for a water cluster as large as a 40-mer, there is still a substantial overlap on the energy distribution between $T = 200$ and 300 K (see Figure 1), which allows a straightforward concatenation of the density-of-state histograms. Therefore, very few simulations (in most cases, two simulations: one at the lower end and the other at the higher end of the temperature range to be investigated) are required to construct the whole histogram that accounts well for those energy states critical to this region of conditions. Furthermore, it should be pointed out that computation of this histogram does not add extra computational burden as the energy calculation is performed for each Monte Carlo move. With the availability of the density-of-state histogram $\Omega_n(E)$, the nucleation free energy formation of the n-mer, ΔG_n^*, at a standard state of $n_v^* = 1$ molecule per Å^3 (as the gas-phase chemical potential or

equivalently the monomer density is often expressed in this unit), can be obtained in the following equation:

$$\Delta G_n^* = -k_B T \ln[\int \Omega_n(E)\, e^{-E/k_B T}\, dE] \quad (2)$$

The nucleation free energy formation of the *n*-mer at any other given gas-phase chemical potential or monomer density n_v can then be determined by applying[24−26]

$$\Delta G_n = \Delta G_n^* - (n-1)k_B T \ln(n_v/n_v^*) \quad (3)$$

which can be related to the cluster size distribution as follows:

$$P(n)/P(1) = \exp(-\Delta G_n/k_B T) \quad (4)$$

3. Molecular Models and Simulation Details

All the water force fields selected in this study belong to the TIP4P family that were shown to reproduce well the density and energy of liquid water at ambient conditions. These include the original nonpolarizable TIP4P model[34] and the polarizable TIP4P−FQ,[35] TIP4P-pol2,[36] and TIP4P-pol3[36] models. In the latter three polarizable force fields, the instantaneous molecular charge distribution is described by three partial charges that are allowed to fluctuate in response to environmental changes to capture the important polarization effects present in water systems (i.e., enhanced molecular dipole moment going from the vapor to the liquid phase). For example, in these polarizable force fields, the dipole moment of the water monomer is set to the correct experimental value, 1.85 D, in contrast to the constant molecular dipole moment of 2.18 D used for the nonpolarizable TIP4P force field in all environments (e.g., not affected by phase changes or location near interfaces or ionic solutes). The two TIP4P-pol models incorporate an additional coupling between the Lennard-Jones interaction parameters for a pair of oxygen sites and their partial charges. This coupling has been shown to improve significantly the accuracy for reproducing the properties of small water clusters.[36] Furthermore, the TIP4P-pol2 model is known to yield an excellent real space representation of the experimentally obtained X-ray structure factor of liquid water over a temperature range from 275 to 350 K at a constant pressure of 101 kPa.[37]

It needs to be emphasized here that all four members of the TIP4P family investigated here are empirical force fields for which the parameters have been determined by fitting classical simulation data directly to experimental data. Therefore, these empirical force fields do implicitly include all quantum effects. Thus, it would be inconsistent to explicitly account for quantum effects in the calculation of nucleation free energy barriers, coexistence properties or second virial coefficients.

A. Nucleation Free Energy (NFE) Profiles. For computational efficiency, the grand-canonical version of the nucleation algorithm[24−26] was used, in which the interactions between the selected cluster and the gas phase are neglected. As demonstrated previously,[25] this is a valid approximation for the low-temperature, low-density cases of interest in this work. A simple Stillinger-type cluster criterion was adopted in this study, that is, a cluster is defined as a group of molecules of which every molecule has at least one neighbor in the group that satisfies a certain threshold, i.e., with an oxygen−oxygen distance below 5 Å (or a pair interaction energy below $-240k_B$ K, see below). Two sets of grandcanonical ensemble nucleation simulations were carried out for each force field, one at 200 K and the other at 300 K. The energy histograms were computed with a bin width of $10k_B$ K. Following eq 1, the density of states were obtained from these distributions and were concatenated into one histogram, which was then utilized to interpret the nucleation free energy formation or the equivalent cluster size distributions at other thermodynamic conditions (i.e., at any temperature between 200 and 300 K and at any gas-phase chemical potential) from eqs 2 to 4. A total of 120 particles (combining the fictitious ideal gas phase and the cluster) and production lengths of $\mathcal{O}(10^6)$ Monte Carlo cycles were used for this set of simulations. The type of Monte Carlo move was selected at random according to the following probabilities: 0.2 for particle insertion and deletion moves, and 0.3 for translational and rotational moves. The maximum displacements for translation and rotation are fixed at 0.3 Å and 0.4 radius, respectively.

B. Coexistence Properties. For each water force field, Gibbs ensemble[38−40] Monte Carlo simulations were also carried out to compute the equilibrium properties of the coexisting phases. These simulations were performed at 300 K with a production length of 500 000 Monte Carlo cycles (one cycle consists of *N* attempted moves where *N* is the number of molecules). Systems consisting of 240 particles were used for simulations employing polarizable force fields while 500 particles were used for the TIP4P model. Four different kinds of Monte Carlo moves were used to sample phase space: translations of the center-of-mass, rotations around the center-of-mass, volume exchanges between the two boxes, and CBMC particle swaps between the two boxes. The maximum displacements used for translational, rotational, and volume moves were adjusted to yield acceptance rates of 50%. The frequencies of the swap and volume moves were adjusted to yield approximately one accepted swap and one accepted volume move per 10 Monte Carlo cycles. The remainder of the moves were equally divided between translations and rotations. In addition, isobaric−isothermal ensemble simulations were carried out at 12 different temperatures for liquid water that are equally spaced between 200 and 300 K in terms of $1/T$ (for the Clausius−Clapeyron integration purpose, see later). Each had a production length of 10^6 Monte Carlo cycles for a 500 particle system. Only translational, rotational, and volume moves were used and their frequencies and maximum displacements were adjusted in the same way as described above for the simulations in the Gibbs ensemble. Although these temperatures may be below the melting point (of these models), ice formation is not observed presumably due to the large ice−nucleation barrier and the constraint by the periodic boundary conditions. With the liquid-water energies obtained from these simulations, the molar heats of vaporization ($\Delta\bar{H}$) are computed, which are subsequently used in the Clausius−Clapeyron integration to evaluate the saturated vapor pressure p_{sat} (or the equivalent vapor-phase density ρ_{vap}^{sat}) at any temperature below 300 K using the following formula:[41,42]

$$d\ln(p) = -\frac{\Delta\bar{H}}{R} d\frac{1}{T} \quad (5)$$

where *R* is the molar gas constant. It should be noted that in deriving the Clausius−Clapeyron integration (eq 5) the saturated vapor-phase is assumed to be an ideal gas and the liquid phase volume is completely ignored. These are appropriate assumptions since both p_{sat} and ρ_{vap}^{sat} are really low. For example, even at the highest value of $T = 300$ K, ρ_{vap}^{sat} is already more than 4 orders of magnitude smaller than the liquid-phase density and p_{sat} is only a few kPa. Some additional Gibbs ensemble Monte Carlo simulations were carried out using the TIP4P force field at temperatures below 300 K to check the accuracy of the vapor-phase densities obtained from the Clausius−Clapeyron integration procedure.

With the coexistence properties, the supersaturation S can be defined. In principle, this property is given by

$$S_{\text{real}} = \exp[(\mu - \mu_{\text{sat}})/k_{\text{B}}T] \quad (6)$$

where μ and μ_{sat} are the chemical potentials for the supersaturated and saturated vapor, respectively. However, for an ideal gas it is common to replace the above definition by a simple pressure ratio p/p_{sat} (or the equivalent gas-phase density ratio $n_{\text{v}}/n_{\text{v}}^{\text{sat}}$). This mechanical-property based term S_{ideal} can be more conveniently calculated from the simulations. As shown previously,[25] the use of S_{ideal} is appropriate for low-density gas phases. For example, for an *n*-heptane system at $T = 275.5$ K and a vapor pressure of 3.3 kPa using the TraPPE-UA force field[43] it was previously found that S_{ideal} deviates from S_{real} by less than 2%, which is well within the statistical uncertainties for the estimated coexistence properties (such as the saturated vapor pressure/density, see later).

C. Nucleation Rates. The nucleation barrier heights ΔG^* obtained from the nucleation free energy calculations can be converted into the corresponding nucleation rates through[44]

$$J = J_0 \exp(-\beta\Delta G^*) = \frac{\rho_{\text{vap}}^{\ 2}}{\rho_{\text{liq}} S}\left(\frac{2\gamma}{\pi m}\right)^{1/2} \exp(-\beta\Delta G^*) \quad (7)$$

where J_0 is the traditional classical prefactor corrected by a factor of $1/S$, ρ_{vap} and ρ_{liq} are the densities of the supersaturated vapor and of the liquid phase at coexistence, respectively, γ is the surface tension, and m is the molecular mass. Most of these terms were taken from the simulations except γ, which was estimated from the following equation:[16]

$$\gamma\ (\text{mN/m}) = 93.6635 + 0.009133 \times T - 0.000275 \times T^2 \quad (8)$$

The above equation was fitted to the experimental surface tension. Although the difference between the experiment results and the model predictions on surface tension can be quite large (e.g., at 298.15 K the calculated value is 56 mN/m for the TIP4P model,[45] compared to the experimental data of 72 mN/m[46]), the nucleation barrier-associated term $\exp(-\beta\Delta G^*)$ is expected to dominate the accuracy in the determination of the nucleation rate.

D. Second Virial Coefficients. The second virial coefficient, $B_2(T)$, is given by[47,48]

$$B_2(T) = -2\pi \int [\langle \exp[-U_{\text{inter}}(r_{12})/k_{\text{B}}T] \rangle_{\alpha_1,\alpha_2} - 1] r_{12}^{\ 2}\, \text{d}r_{12} \quad (9)$$

where $U_{\text{inter}}(r_{12})$ is the intermolecular dimer energy when the distance between the COM of molecules 1 and 2 is r_{12}, and $\langle \cdots \rangle_{\alpha_1,\alpha_2}$ denotes the canonical ensemble average sampled over conformations of molecules 1 and 2, which are Boltzmann weighted solely on their intramolecular energies by utilizing two simulation boxes.[43] A million conformations were utilized to calculate the ensemble average, and the integral was evaluated from 0 to 100 Å with a 0.04 Å step size.

E. Adiabaticity in Simulations Employing Polarizable Force Fields. For simulations with polarizable force fields, the adiabatic separation of the nuclear and electronic degrees of freedom (imposed by the Born−Oppenheimer requirement) is a critical issue. For simulations in the *NpT* ensemble, this was achieved by the adiabatic and nuclear electronic sampling Monte Carlo (ANES-MC) algorithm with an appropriate choice of $T_{\text{elec}} = \infty$ and $R_{\text{elec}} = 1$.[36,49−51] Whereas for simulations in the Gibbs and grandcanonical ensembles, this was satisfied strictly through the matrix-minimization scheme.[50] For these simulations particle swaps are the dominant type of moves, which result in a substantial perturbation of the electronic environment, and a large R_{elec} would be needed if the ANES-MC algorithm were used.

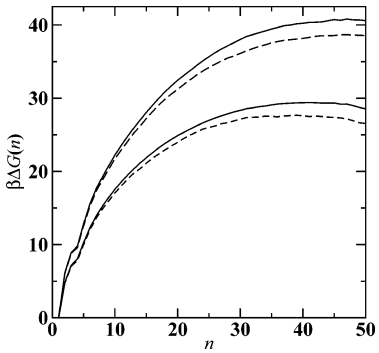

Figure 2. Comparison of the nucleation free energy profiles obtained at $T = 230$ K and $n_v = 4.2 \times 10^{-8}$ Å^{-3} (upper two lines) and $T = 260$ K and $n_v = 5 \times 10^{-7}$ Å^{-3} (lower two lines) calculated using distance-based or energy-based cutoffs (solid and dashed lines, respectively).

F. Treatment of Long-Range Interactions. For Gibbs and isobaric−isothermal ensemble simulations, a spherical potential truncation at $r_{\text{cut}} = 9$ Å with analytical tail corrections was used for the Lennard-Jones interactions and the Ewald-sum technique was employed to account for the long-range electrostatic interactions.[52] For the grandcanonical-ensemble nucleation simulations, all the pair interactions were included in the computation of the total energy.

4. Simulation Results and Discussions

A. Influence of the Cluster Criterion on the Nucleation Free-Energy Barrier. As mentioned in section 3.A, a simple distance-based cluster criterion is used for these nucleation simulations. To determine whether the oxygen−oxygen pair distance is a suitable choice for water (a molecule for which the intermolecular interactions are dominated by anisotropic electrostatic forces), a comparison is made between the NFE profiles calculated for the TIP4P model using this criterion and those with an energy-based cutoff (obtained from previous simulations done by us[26]). As shown in Figure 2, using a distance cutoff at 5 Å appears to consistently produce a slightly higher nucleation barrier height increased by about $2k_{\text{B}}T$ compared to an energy cutoff of $-240k_{\text{B}}$ K (where two water molecules are considered to be bound together in one cluster if their pair interaction energy is less than $-240k_{\text{B}}$ K). The magnitude of this shift is similar to those observed previously by changing the value of the energy cutoff.[25] Overall, the NFE curve is not very sensitive to the choice of the cutoff criterion. This agrees with a very recent simulation study on water nucleation.[18] Thus, we selected the distance cutoff as it is very convenient to implement for the aggregation-volume-bias Monte Carlo framework (i.e., the associating region for the AVBMC swap moves was bound by a radius of 5 Å between the oxygens, the same distance used for the Stillinger-type cluster criterion).

B. Comparison of the Nucleation Behavior Observed in Simulation and Experiment. As the nucleation pulse experimental measurements were carried out under isobaric−isothermal conditions, a fair comparison between the simulation and the experiment should be, in principle, made using the same absolute pressure but only provided the simulation model is sufficiently accurate. However, it was pointed out previously that even simple equilibrium properties such as the vapor−liquid coexistence curves pose a grand challenge for water force

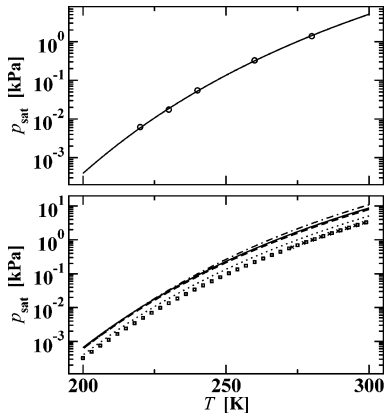

Figure 3. Saturated vapor pressures, p_{sat}, as function of the temperature. (Top) Comparison of p_{sat} for the TIP4P model calculated from the Clausius−Clapeyron integration (solid line) and the direct Gibbs ensemble Monte Carlo simulations (circles). (Bottom) Comparison of p_{sat} between experimental data[54] (crosses), the Wagner equation of state[53] (squares), and the simulation data for the TIP4P, TIP4P-pol2, TIP4P-pol3, and TIP4P−FQ models denoted by dotted, dashed, solid, and dash−dotted lines, respectively.

fields.[36] At least none of the current water force fields has been shown to be able to yield good agreement for the coexistence densities and liquid structure over the entire temperature range from the triple point to the critical point. Thus, additional simulations in the Gibbs and isobaric−isothermal ensembles combined with the Clausius−Clapeyron equation were used to compute the coexistence properties and to allow for simulations for the same supersaturation range as investigated experimentally.

Plotted in Figure 3 are the saturated vapor pressures as function of the temperature obtained from the simulations and the experiments. Apparently for the temperature range of our interest (200−300 K), the water vapor phase has really low vapor pressures and densities, thus allowing the straightforward application of the Clausius−Clapeyron integration. Indeed, the results interpreted from this method agree well with those calculated from the additional Gibbs ensemble simulations which were carried out at temperatures below 300 K (see Figure 3). For example, for the TIP4P force field, the following pressures (in unit of Pa) were obtained from the Gibbs ensemble simulations: 6.2 ± 0.4 (220 K); 17.5 ± 0.9 (230 K); 55.1 ± 1.8 (240 K); 328 ± 12 (260 K); and 1385 ± 33 (280 K) as compared to: 5.9 (220 K); 18.6 (230 K); 52.5 (240 K); 319 (260 K); and 1432 (280 K) extrapolated from the Clausius−Clapeyron integration. The differences are of similar magnitude as the statistical uncertainties. It should be noted that the applicability of the Gibbs ensemble technique to these ultralow-temperature phase equilibrium calculations was enabled by advanced CBMC techniques,[29−31] which allow successful particle exchanges between the vapor and liquid phase even far below room temperature for water (0.015 swap moves were accepted per Monte Carlo cycle at $T = 220$ K when 50% of the moves are swaps, compared to 0.17 accepted moves at 300 K when swaps are attempted 20% of the time); albeit larger relative uncertainties were found for the values obtained at lower temperatures for equal production length (10^6 Monte Carlo cycles here). On the contrary, the Clausius−Clapeyron integration avoids this technical difficulty. Furthermore, using precise heats of vaporization data and a simple integration scheme allows us to evaluate the saturated vapor pressure at any temperature in the range of interest.

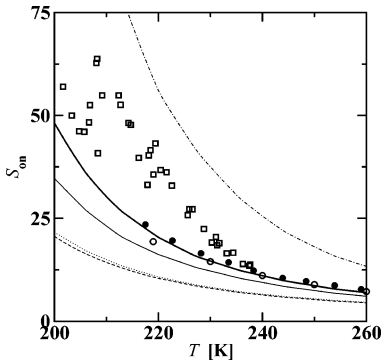

Figure 4. Onset-supersaturation, S_{on} ($= n_v/n_v^{sat}$ yielding a constant nucleation rate), as function of temperature. The experimental data obtained by Wölk and Strey[16] and by Viisanen, Strey, and Reiss[11] for a constant nucleation rate $J = 10^7$ cm^{-3} s^{-1}, and by Peeters et al.[17] for a nucleation rate ranging from $J = 10^8$−10^{10} cm^{-3} s^{-1} are shown as open circles, filled circles, and open squares, respectively. The simulation data for constant $J = 10^7$ cm^{-3} s^{-1} computed for the TIP4P, TIP4P-pol2, TIP4P-pol3, and TIP4P−FQ models are shown as thin dotted, dashed, solid, and dash−dotted lines, respectively. The thicker solid curve denotes calculated data for the TIP4P-pol3 model and a higher nucleation rate of $J = 10^{10}$ cm^{-3} s^{-1}.

Also plotted in Figure 3 is the equilibrium vapor pressure used by Wölk and Strey[16] for the interpretation of their experimental nucleation results. They utilized an empirical equation of state (obtained by Wagner[53]) to generate the saturated vapor pressure of supercooled liquid water below its triple point temperature as follows:

$$p_{sat}^{exp}\,(\mathrm{Pa}) = \exp(77.34491 - 7235.42465/T - 8.2 \ln T + 0.0057113T) \quad (10)$$

As shown in Figure 3, this equation reproduces well the experimental water vapor pressure[54] over the near-freezing temperature range. However, all water force fields utilized in this study give saturated water vapor pressures that are significantly higher than either the real experimental values or the data generated from eq 10 over the entire temperature range. The nonpolarizable TIP4P model actually yields more accurate vapor pressures than the polarizable models, but still its deviation from the experimental data can be as large as 40%. Therefore, the comparison of the nucleation results is only performed on a relative supersaturation scale. A simple definition of n_v/n_v^{sat} is used here to compute the supersaturation (S_{ideal}). The deviation of this from S_{real} is expected to be small (1−2%) for the low-density/pressure cases, which is within the statistical uncertainty of the estimated saturated vapor pressure/density and also well below the differences between the experimental data and the various force field predictions on the nucleation results (see below).

As mentioned in the Introduction, experimental difficulties can sometimes lead to disagreements on the nucleation behavior observed for water. In particular, the two latest experimental measurements done by two separate groups show rather different temperature-dependence of the nucleation rates over the temperature range from 200 to 260 K.[16,17] This difference is highlighted by a comparison of the measured onset supersaturation (see Figure 4). Clearly the experimental data obtained by van Dongen and co-workers[17] show a much stronger temperature-dependence compared to those obtained by Wölk and Strey[16] over the temperature range between 215 and 240 K. In addition, a plateau (or maybe substantial scatter) was found by van Dongen and co-workers[17] below 215 K, followed by a

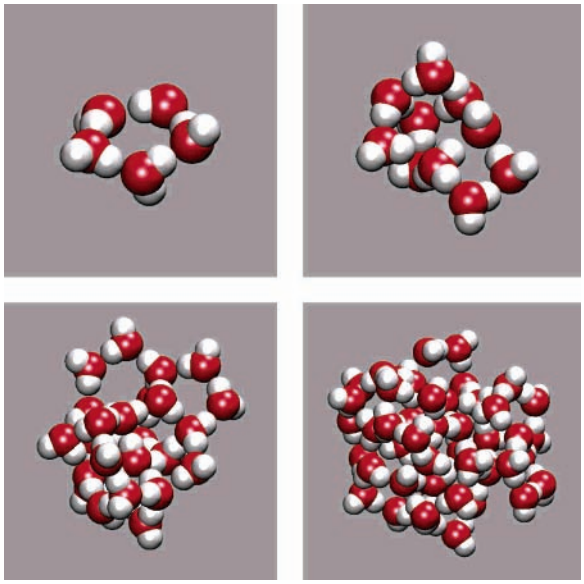

Figure 5. Snapshots of water clusters (consisting of 5, 10, 25, or 50 molecules) obtained at $T = 200$ K using the TIP4P-pol3 model. At $n_v = 8.38 \times 10^{-9}$ Å^{-3} (the condition at which the calculated nucleation rate is equal to 10^7 cm^{-3}s^{-1}), the size of the critical cluster (a transition structure located at the saddle point of the nucleation free energy profile) is approximately 25 molecules. Oxygens and hydrogens are colored in red and white, respectively.

dip at about 207 K. This peculiar behavior was interpreted as a transition from vapor/liquid to vapor/solid nucleation. Wölk and Strey did not extend their experimental measurement below 215 K, and it is not possible to infer from their data whether a plateau might appear at lower temperature. However, it should be noted that there is little indication in the data of Wölk and Strey that points to a dramatic increase in experimental scatter at the lowest temperatures. Thus, the smoothness of their data points against $T \simeq 215$ K being in the vicinity of a phase transition.

The simulation results obtained from the four different force fields are also plotted in Figure 4. The simulation data are very precise (small statistical uncertainties) but the spread between data computed for different force fields is much larger than the difference between the two experimental data sets. This large spread is an indication of the sensitivity of the nucleation results to the force field parameters, which was also observed in previous simulation studies.[18,55] However, the data for these TIP4P-type force fields does not support a sudden transition at the low temperature region. Instead all curves display a rather smooth temperature-dependence of the onset supersaturation. In addition, neither visual inspection nor structural analysis (radial distribution functions, translational and orientational order parameters) for the critical nuclei give any clear evidence that would support the ice crystallite formation. In fact, the critical clusters are so small that the majority of water molecules appear at the cluster−vapor surface. There is little bulk phase to allow for a formation of the ice crystallite inside these critical clusters. The water molecules are simply arranged in a disordered, hydrogen-bonded chainlike structure at the cluster-vapor surface (see Figure 5). It should also be noted that the simulation curves appear to be in parallel with Strey and co-worker's data. Although they show significant deviations, they seem to be uniform over the entire temperature range. For example, the TIP4P model underestimates the onset supersaturation consistently by about 40%. This agrees with early simulation findings that the TIP4P model produces a temperature dependence

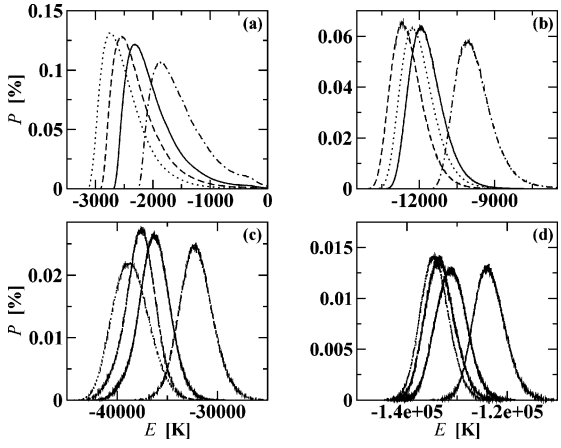

Figure 6. Normalized energy distributions obtained at $T = 200$ K for (a) dimer, (b) tetramer, (c) decamer, and (d) triacontamer (30-mer) obtained using the TIP4P (dotted lines), TIP4P-pol2 (dashed), TIP4P-pol3 (solid), and TIP4P-FQ (dash−dotted) models.

consistent with Strey and co-worker's data except that it constantly overestimates the nucleation rate.[18,56]

Among the four different force fields selected in this study, the TIP4P-pol3 model clearly outperforms the others, with a constant underestimation of the on-set supersaturation by about 10%, compared to the experimental results by Wölk and Strey.[16] This deviation in the on-set supersaturation corresponds to a nucleation rate difference of roughly 3 orders of magnitude. As shown in Figure 4, the onset supersaturation plot obtained for this model at a constant nucleation rate of $J = 10^{10}$ cm^{-3} s^{-1} nearly coincides with the experimental data of Wölk and Strey[16] at $J = 10^7$ cm^{-3} s^{-1}. It should be pointed out that the experimental results obtained by van Dongen and co-workers[17] actually scatter over the range between $J = 10^8$ and 10^{10} cm^{-3} s^{-1}. Nevertheless, the deviation between these two sets of experimental data on the onset supersaturation varies from less than 5% at 237 K to nearly 80% at 217 K, for which the difference in nucleation rates is an insufficient explanation.

For the nonpolarizable TIP4P model, it is straightforward to rationalize its underestimation of the onset supersaturation. Since the fixed electronic charges are parametrized to reproduce the thermodynamic properties of liquid water at the room temperature, they implicitly include the manybody polarization effects of this particular thermodynamic state. In nucleation processes, however, multiple phases (clusters with different sizes) coexist that are characterized by varying degrees of many-body effects and cannot be appropriately accounted for by a fixed-charge model. In particular, considering the small sizes of the critical nuclei, most water molecules are located at the vapor−cluster surface (see Figure 5), an environment halfway between the vapor and the bulk phase. Therefore, the many-body polarization effects present in these clusters are expected to be larger than the vapor but smaller than the bulk phase, i.e., akin to those found at vapor−liquid interfaces.[57] On the other hand, using those charges that correspond to the bulk phase environment for these small clusters would lead to an overestimation of the many-body effects and more negative energies. Indeed, numerous theoretical studies that are centered around the development of water force fields have pointed out that nonpolarizable water models tend to overestimate the magnitude of the minimum energies for small clusters.[36,58,59] This was also observed directly throughout the nucleation simulations. As shown in Figure 6, the cluster energy distributions for the TIP4P model, in general, are shifted to the more negative side compared to the polarizable models. Although exceptions were noticed for tetramer to

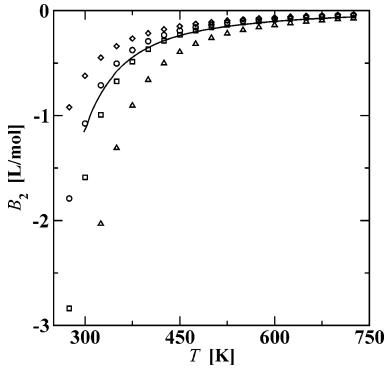

Figure 7. Comparison of the second virial coefficients, B_2, calculated for the TIP4P (triangles), TIP4P-pol2 (squares), TIP4P-pol3 (circles), and TIP4P−FQ (diamonds) models. The solid line represents the experimental data.[60]

heptamer for which the TIP4P-pol2 model could yield more negative energy distributions than the TIP4P model, this trend is more consistent for higher cluster sizes. Since more negative energies favor cluster formation, we would expect lower nucleation free energies and nucleation barrier heights or higher nucleation rates for the TIP4P model. This is consistent with the fact that it underestimates the onset supersaturation. On the contrary, the energy distributions yielded by the polarizable TIP4P-FQ model are shifted significantly to the more positive side, which explains the substantial overestimation of the onset supersaturation. Such a correlation between the nucleation results and the cluster energies was also observed previously.[18,55]

The experiments by Wölk and Strey[16] on the homogeneous nucleation of H_2O and D_2O also indicated that nucleation properties are extremely sensitive to molecular interactions. The nucleation rates for these two seemingly similar molecular systems were found to differ by a factor of 2500. Considering that a much larger variation on the molecular interactions is present between the different water force fields, it is not surprising to observe a wide spread of the calculated nucleation results (although all of the force fields employed yield similar thermodynamic properties for liquid water at room temperature and all the polarizable models also give the right dipole moment for the water monomer). It is interesting to note that the polarizable TIP4P−FQ model yields significantly less accurate nucleation properties than the nonpolarizable TIP4P model, supporting an early simulation finding that polarizable force fields are not necessarily better (or more transferable) for the prediction of nucleation properties than the nonpolarizable force fields.[18] On the other hand, it is encouraging to see that the polarizable TIP4P-pol3 model produces the best nucleation results (see Figure 4 and previous discussions). Previously this force field has been shown to yield very good binding energies for water clusters (from dimer to hexamer) compared to the ab initio calculations.[36]

Furthermore, the second virial coefficients, B_2, were computed to assess the accuracy of the force field for the smallest cluster at finite temperatures. Plotted in Figure 7 is a comparison of B_2 between the force field calculations and the experimental data.[60] The B_2 values display the same trend as observed in the onset supersaturation plot. Whereas the TIP4P model yields more negative B_2 (due to the overestimate of the dimer energies), the TIP4P−FQ model underestimates B_2. In contrast, the two TIP4P-pol models produce B_2 values that are very close to the experimental data. The consistently better performance of the TIP4P-pol models for these properties not only suggests that there is an intimate connection between these properties and nucleation behavior but also implies a potential strategy leading

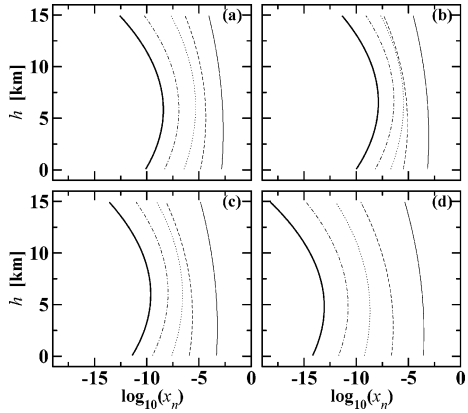

Figure 8. Mole fractions for clusters from dimer up to hexamer (right to left) as function of altitude calculated for the (a) TIP4P, (b) TIP4P-pol2, (c) TIP4P-pol3, and (d) TIP4P−FQ models. The mole fractions for dimer to hexamer are shown as solid, dashed, dotted, dash−dotted, and thick solid lines, respectively.

to a water force field with better transferability. In particular, nucleation properties are ideal for a stringent test/development of transferable many-body force fields since they are experimentally available and are shown to be sensitive to molecular interactions. In addition, the states involved in nucleation processes are sufficiently diverse to mimic the heterogeneous environments experienced by many other important systems, e.g., biological molecules.

C. Aggregation of Water Cluster in the Atmosphere. Using the histogram-reweighting approach, it is straightforward to convert through eq 4 the nucleation free energy data to the concentrations of water clusters under homogeneous atmospheric conditions. Thereby allowing us to address the important atmospheric question of the effect of larger water clusters on the solar radiation balance. Following Evans and Vaida's work,[19] the temperature and monomer density of water in the atmosphere were approximated by the empirically derived equations (which were fitted to the experimental data for an elevation less than 15 km)[61,62]

$$T(h) = 289\ \mathrm{e}^{-0.021h} \tag{11}$$

$$\log_{10}(\rho_1(h)) = -(0.11h)^2 + 0.0137h + 17.315 \tag{12}$$

where the elevation h and the monomer density $\rho_1(h)$ are in units of km and molecules per cm^3, respectively. From eq 11, the temperature, $T(h)$, at any elevation below 15 km falls within the range of 200 to 300 K (i.e., $T(h) = 289$ K at sea-level and 210.9 K at $h = 15$ km). Thus, the density of states constructed from the nucleation simulations performed at $T = 200$ and 300 K can be directly applied here in the calculation of the water cluster concentrations through the histogram-reweighting technique (i.e., eqs 2−4).

Plotted in Figure 8 are the mole fractions of water clusters (from dimer to hexamer) as function of altitude. Again, a large spread of the simulation results is observed for the four different force fields. In general, the nonpolarizable TIP4P model predicts higher mole fractions and the polarizable TIP4P−FQ model gives significantly lower cluster concentrations, whereas the TIP4P-pol models yield some values in between. This is consistent with the nucleation results and the energy distributions of the water clusters. An additional difference is that the TIP4P-pol models yield relatively similar concentrations for trimers and tetramers. The tetramer possesses significantly less ring stress and it has been shown previously[36] that in particular the

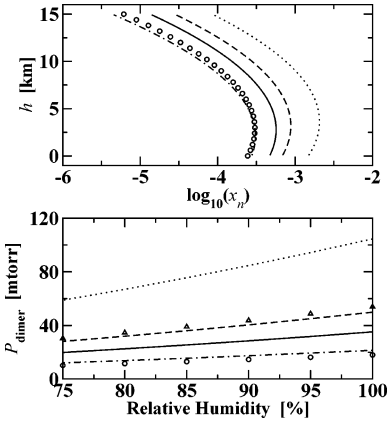

Figure 9. (Top) Comparison of the dimer mole fraction as function of altitude predicted by Evans and Vaida[19] (circles) with the simulation data obtained using the TIP4P, TIP4P-pol2, TIP4P-pol3, and TIP4P−FQ model denoted by dotted, dashed, solid, and dash−dotted lines, respectively. (Bottom) Comparison of the dimer partial pressure as function of relative humidity at $T = 298$ K predicted by Goldman et al.[21] (triangles) with the results calculated using the TIP4P, TIP4P-pol2, TIP4P-pol3, TIP4P-FQ, and Evans and Vaida's model. Symbols as in the top panel. The water monomer vapor pressure was computed using the same scheme described in ref 21.

TIP4P-pol2 model is able to reproduce the large jump in the cluster binding energy from trimer (−66 kJ/mol) to tetramer (−120 kJ/mol) obtained in high-level ab initio calculations.[63] In contrast, the cluster concentrations determined by Evans and Vaida[19] and calculated here for the TIP4P and TIP4P−FQ models show substantially more even spacing between different aggregate sizes. This is presumably related to the fact that these simpler models do not account for additional stabilization of small cyclic clusters beyond tetramer.

For the atmospherically most relevant dimer,[19] it appears (see Figure 9) that with the exception of the fixed-charge TIP4P model (that was fitted purely to bulk data and thus its enhanced dipole moment leads to overestimated binding energies particularly for small clusters), the dimer concentrations obtained for the TIP4P−FQ and TIP4P-pol models fall within the range between the results produced by the model of Evans and Vaida (that was fitted approximately to dimer properties, such as experimental dimerization equilibrium constant and the second virial coefficient) and those predicted by Goldman et al. using a sophisticated force field that was directly fitted to high-resolution spectroscopic data of the water dimer.[21] On the contrary, the predictions from the Evans and Vaida's theory[19] for clusters larger than trimers are substantially smaller than those found for the TIP4P-pol models presumably because a dimer potential neglects the favorable manybody polarization effects present in the larger clusters. However, the main conclusion of Evans and Vaida that the atmospheric concentration of larger clusters is very low (e.g., the mole fraction of hexamers is only about 10^{-10}) is clearly supported by the simulation of this work.

Finally, the AVUS−HR approach allows for an easy extension of the prediction of cluster abundances to larger sizes. As a representative example, the mole fractions of clusters up to pentacontamer (50-mer) computed for the TIP4P-pol3 model (that gives the best agreement with the nucleation data by Wölk and Strey) are shown in Figure 10. It can safely be assumed that aggregates with abundances near an inverse google are only of purely computational interest.

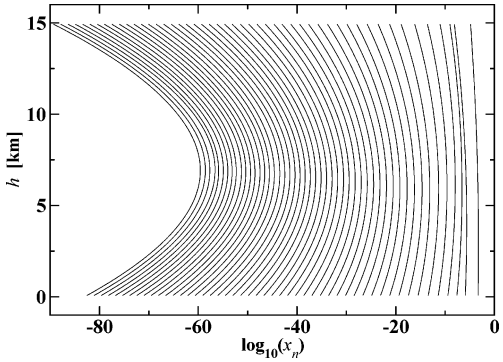

Figure 10. Mole fractions for clusters from dimer up to pentacontamer (50-mer, right to left) as function of altitude calculated for the TIP4P-pol3 model.

5. Conclusions

In conclusion, the histogram-reweighting technique was integrated with a recently developed nucleation simulation method to form the AVUS-HR (aggregation-volume-bias Monte Carlo with umbrella sampling and histogram reweighting) approach. Through the use of AVUS-HR, it becomes possible to carry out only two simulations (one at 200 K and the other at 300 K) to produce the nucleation free energies over a wide range of thermodynamic conditions. AVUS-HR was applied here to investigate the nucleation behavior of water using fixed-charge and polarizable force fields belonging to the TIP4P family. The large spread of the results calculated for the different force fields indicates that the nucleation properties are extremely sensitive to the details of molecular interactions. Despite this large spread, however, all force fields employed in this investigation do not show any sign of ice nucleation and a temperature-dependence of onset supersaturation that is in fair agreement with the experimental data by Wölk and Strey.[16] In addition, a systematic trend was observed for the nucleation properties produced by these force fields that parallels with the energy distributions of the water clusters, the second virial coefficient, and the minimum binding energies of the water clusters. In particular, the TIP4P-pol models show consistently better performance than the TIP4P and TIP4P-FQ models for these properties, implying that a proper inclusion of the many-body polarization effects is necessary for achieving a better transferability. In this regard, nucleation properties are ideal for a stringent test/development of transferable many-body force fields.

Furthermore, the calculated nucleation free energy data were also converted to water cluster concentrations to investigate the homogeneous aggregation of water molecules in the atmosphere. The calculated mole fractions of water clusters show a significant spread between different force fields but all data point to very low abundances of larger clusters with the mole fraction of the hexamer being only about 10^{-10}, a number probably too low to influence the solar radiation, and the mole fraction of the pentacontamer falling around 10^{-100}.

Acknowledgment. We thank Ken Leopold, Bruce Garett, Greg Schenter, Shawn Kathmann, Veronica Vaida, Howard Reiss, Kwang Jin Oh, and Barbara Hale for many stimulating discussions. Financial support from the National Science Foundation CTS-0138393 (J.I.S.), CHE-0205146 (M.L.K.), CHE-0448918 (B.C.), and LSU start-up funds (B.C.) is gratefully acknowledged. Part of the computer resources were provided by the Minnesota Supercomputing Institute and the Center for Computation and Technology at LSU (SuperMike).

Note Added in Proof. After this manuscript was submitted, we learned about related work by Dunn et al.[64] who used electronic structure calculations with complete basis set methods to investigate the thermodynamics of small water clusters. At a temperature of 373 K, these electronic structure calculations yield an enthalpy of dimerization of about −13 kJ/mol, in good agreement with an experimental thermal conductivity measurement that yields a dimerization enthalpy of -15 ± 2 kJ/mol.[65] In comparison, the AVUS-HW calculations yield −16.7, −9.8, −13.7, and −12.1 kJ/mol, for the TIP4P, TIP4P-FQ, TIP4P-pol2, and TIP4P-pol3 models, respectively. Furthermore, a water dimer concentration of approximately 6×10^{14} molecules/cm^3 was recently obtained from near-infrared spectroscopic measurements for saturated air at $T = 292.4$ K.[66] For the same condition, the calculations presented here give 21, 4.0, 9.6, and 6.7×10^{14} for the TIP4P, TIP4P-FQ, TIP4P-pol2, and TIP4P-pol3 models, respectively (see also Figure 9).

References and Notes

(1) Wilson, C. R. T. *Philos. Trans. R. Soc. London. Ser. A* **1897**, *189*, 265.
(2) Volmer, M.; Flood, H. Z. *Phys. Chem. A* **1934**, *190*, 273.
(3) Sander, A.; Damköhler, G. *Naturwissenschaften* **1943**, *31*, 460.
(4) Wegener, P.; Lundquist, G. *J. Appl. Phys.* **1951**, *22*, 233.
(5) Courtney, W. G. *J. Chem. Phys.* **1961**, *35*, 2249.
(6) Katz, J. L.; Ostermier, B. *J. Chem. Phys.* **1967**, *47*, 478.
(7) Allen E.; Kassner, J. L. *J. Colloid Interface Sci.* **1969**, *30*, 81.
(8) Heist, R.; Reiss, H. *J. Chem. Phys.* **1973**, *59*, 865.
(9) Miller, R.; Anderson, R. J.; Kassner, J. L.; Hagen, D. E. *J. Chem. Phys.* **1983**, *78*, 3204.
(10) Peters, F.; Paikert, B. *Exp. Fluids* **1989**, *7*, 521.
(11) Vissanen, Y.; Strey, R.; Reiss, H. *J. Chem. Phys.* **1993**, *99*, 4680.
(12) Vissanen, Y.; Strey, R.; Reiss, H. *J. Chem. Phys.* **2000**, *112*, 8205.
(13) Wölk, J.; Vissanen, Y.; Strey, R. In *Proceedings of the 15th International Conference on Nucleation and Atmospheric Aerosols*; Hale, B. N., Kulmala, M., Eds.; American Institute of Physics: Woodbury, NY, 2000; p 7.
(14) Schmitt, J. L.; Brunt, K. V.; Doster, G. J. In *Proceedings of the 15th International Conference on Nucleation and Atmospheric Aerosols*; Hale, B. N., Kulmala, M., Eds.; American Institute of Physics: Woodbury, NY, 2000; p 51.
(15) Mikheev, V. B.; Laulainen, N. S.; Barlow, S. E.; Pervukhin, V. V. In *Proceedings of the 15th International Conference on Nucleation and Atmospheric Aerosols*; Hale, B. N., Kulmala, M., Eds.; American Institute of Physics: Woodbury, NY, 2000; p 71.
(16) Wölk, J.; Strey, R. *J. Phys. Chem. B* **2001**, *105*, 11683.
(17) Peeters, P.; Gielis, J. J. H.; van Dongen, M. E. H. *J. Chem. Phys.* **2002**, *117*, 5647.
(18) Merikanto, J.; Vehkamäki, H.; Zapadinsky, E. *J. Chem. Phys.* **2004**, *121*, 914.
(19) Evans, G. T.; Vaida, V. *J. Chem. Phys.* **2000**, *113*, 6652 and references therein.
(20) Paul, J. B.; Collier, C. P.; Saykally, R. J.; Scherer, J. J.; Okeefe, A. *J. Phys. Chem. A* **1997**, *101*, 5211.
(21) Goldman, N.; Leforestier, C.; Saykally, R. J. *J. Phys. Chem. A* **2004**, *108*, 787.
(22) Wilding, N. B. *Phys. Rev. E* **1995**, *52*, 602.
(23) Potoff, J. J.; Panagiotopoulos, A. Z. *J. Chem. Phys.* **1998**, *109*, 10914.
(24) Chen, B.; Siepmann, J. I.; Oh, K. J.; Klein, M. L. *J. Chem. Phys.* **2001**, *115*, 10903.
(25) Chen, B.; Siepmann, J. I.; Oh, K. J.; Klein, M. L. *J. Chem. Phys.* **2002**, *116*, 4317.
(26) Chen, B.; Siepmann, J. I.; Klein, M. L. *J. Am. Chem. Soc.* **2003**, *125*, 3113.
(27) Chen, B.; Siepmann, J. I. *J. Phys. Chem. B* **2000**, *104*, 8725.
(28) Chen, B.; Siepmann, J. I. *J. Phys. Chem. B* **2001**, *105*, 11275.
(29) Siepmann, J. I.; Frenkel, D. *Mol. Phys.* **1992**, *75*, 59.
(30) Frenkel, D.; Mooij, G. C. A. M.; Smit, B. *J. Phys.: Condens. Matter* **1992**, *4*, 3053.
(31) Martin, M. G.; Siepmann, J. I. *J. Phys. Chem. B* **1999**, *103*, 4508.
(32) Torrie, G. M.; Valleau, J. P. *Chem. Phys. Lett.* **1974**, *28*, 578.
(33) Metropolis, N.; Rosenbluth, A. W.; Rosenbluth, M. N.; Teller, A. H.; Teller, E. *J. Chem. Phys.* **1953**, *21*, 1087.
(34) Jorgensen, W. L.; Chandrasekhar, J.; Madura, J. D.; Impey, R. W.; Klein, M. L. *J. Chem. Phys.* **1983**, *79*, 926.
(35) Rick, S. W.; Stuart, S. J.; Berne, B. J. *J. Chem. Phys.* **1994**, *101*, 6141.
(36) Chen, B.; Xing, J.; Siepmann, J. I. *J. Phys. Chem. B* **2000**, *104*, 2391.
(37) Hura, G.; Russo, D.; Glaeser, R. M.; Head-Gordon, T.; Krack, M.; Parrinello, M. *Phys. Chem. Chem. Phys.* **2003**, *5*, 1981.
(38) Panagiotopoulos, A. *Z. Mol. Phys.* **1987**, *61*, 813.
(39) Panagiotopoulos, A. Z.; Quirke, N.; Stapleton, M.; Tildesley, D. J. *Mol. Phys.* **1988**, *63*, 527.
(40) Smit, B.; de Smedt, P.; Frenkel, D. *Mol. Phys.* **1989**, *68*, 931.
(41) McQuarrie, D. A.; Simon, J. D. *Physical Chemistry: A Molecular Approach*; University Science Books: Sausalito, CA, 1997.
(42) Kofke, D. A. *Adv. Chem. Phys.* **1999**, *105*, 405.
(43) Martin, M. G.; Siepmann, J. I. *J. Phys. Chem. B* **1998**, *102*, 2569.
(44) Seok C.; Oxtoby, D. W. *J. Chem. Phys.* **1998**, *109*, 7982.
(45) Chen, B.; Siepmann, J. I.; Klein, M. L. *J. Am. Chem. Soc.* **2002**, *124*, 12232.
(46) Lide, D. A. *CRC Handbook of Chemistry and Physics*; CRC Press: Boca Raton, FL, 1991.
(47) Harismiadis, V. I.; Szeifer, I. *Mol. Phys.* **1972**, *23*, 41.
(48) McQuarrie, D. A. *Statistical Mechanics*; Harper and Row: New York, 1976; p 227.
(49) Martin, M. G.; Chen, B.; Siepmann, J. I. *J. Chem. Phys.* **1998**, *108*, 3383.
(50) Chen, B.; Siepmann, J. I. *Theo. Chem. Acc.* **1999**, *103*, 87.
(51) Chen, B.; Potoff, J. J.; Siepmann, J. I. *J. Phys. Chem. B* **2001**, *105*, 3093.
(52) Allen, M. P.; Tildesley, D. J. *Computer Simulation of Liquids*; Oxford University Press: Oxford, U.K., 1987.
(53) Wagner, P. E. *Aerosol Research III*; Wien 1981, 209.
(54) NIST Chemistry WebBook, http://webbook.nist.gov/chemistry.
(55) Kathmann, S. M.; Schenter, G. K.; Garett, B. C. *J. Chem. Phys.* **2002**, *116*, 5046.
(56) Hale, B. N.; DiMattio, D. In *Proceedings of the 15th International Conference on Nucleation and Atmospheric Aerosols*; Hale, B. N., Kulmala, M., Eds.; American Institute of Physics: Woodbury, NY, 2000; p 31.
(57) Kuo, I.-F. W.; Mundy, C. J. *Science* **2004**, *303*, 658.
(58) Xantheas, S. S.; Burnham, C. J.; Harrison, R. J. *J. Chem. Phys.* **2002**, *116*, 1493.
(59) Burnham, C. J.; Xantheas, S. S. *J. Chem. Phys.* **2002**, *116*, 1500.
(60) Tsonopoulos, C.; Heidman, J. L. *Fluid Phase Equilib.* **1990**, *57*, 261.
(61) Brasseur, G.; Solomon, S. *Aeronomy of the Middle Atmosphere: Chemistry and Physics of the Stratosphere and Mesosphere*, 2nd ed.; Reidel: Dordrecht, The Netherlands, 1986.
(62) Vaida, V.; Daniel, J. S.; Kjaergaard, H. G.; Goss, L. M. Q. J. R. *Meterol. Soc.* **2001**, *127*, 1627.
(63) Gregory, J. K.; Clary, D. C. *J. Phys. Chem.* **1996**, *100*, 18014.
(64) Dunn, M. E.; Pokon, E. K.; Shields, G. C. *J. Am. Chem. Soc.* **2004**, *126*, 2647.
(65) Curtiss, L. A.; Frurip, D. J.; Blander, M. *J. Chem. Phys.* **1979**, *71*, 2703.
(66) Pfeilsticker, K.; Lotter, A.; Peters, C.; Bösch, H. *Science* **2003**, *300*, 2078.